CCIT Report #592 June 2006

Sampling Finite-Support Sobolev Signals and Images

Hagai Kirshner and Moshe Porat

Abstract

Considering finite-support signals, it is shown that the ideal sampling process can be described by means of an orthogonal projection within a Sobolev space. This interpretation is shown to account for non-uniform and for non-ideal sampling schemes as well. It further enables one to derive a minimax approximation scheme for an arbitrary linear bounded functional while utilizing the sampled version of the signal as the only available data. The paper extends and generalizes recent results derived for the infinite-support case, and proposes accordingly applications suitable for the more practical situation of finite-support signals (images) such as approximation of representation coefficients, Fourier transform evaluation and derivative calculations. The new approach offers further insight into the intertwining relationship between the analog and the discrete domains, suggesting improved methods for multi-dimensional signal processing applications.

Sampling Finite-Support Sobolev Signals and Images

I. Introduction

Discrete implementation of continuous-domain operations is widely used in signal and image processing applications. Such discrete schemes process the sampled version of an analog signal, and manipulating it to yield another set of discrete data. The latter is assumed to provide an approximation of the continuous-domain operator acting on the original analog signal. Examples of such cases include numerical implementation of differential operators, combined spaces representation such as the Gabor and wavelets schemes, and classical filtering tasks.

Consider a signal representation scheme for which a single representation coefficient is defined by an $L_2(\Omega)$ inner product. In cases where the sampled version of a signal is the only available data, it is a common practice to approximate this inner product by means of a Riemann type sum. This type of approximation indeed converges, but some regularity constraints are to be imposed on the original continuous-domain functions [1]. Nevertheless, this convergence has not been put in the context of signal representation schemes for which the analysis function is analytically known a priori. Furthermore, uniform ideal sampling is not the only relevant sampling scheme and practical non-ideal acquisition devices may be considered as well. A mathematical framework for describing non-ideal acquisition devices has been recently introduced [2], [3], awaiting to be incorporated in such an approximation scheme.

The Riemann type sum is also evident in the discrete Fourier transform (DFT). Having the sampled version of a signal, the DFT provides a Riemann type sum approximation for the Fourier transform itself at certain frequencies. However, an alternative approximation scheme is called for, with the emphasis on both the sampling process characteristics (such as ideal, non-ideal) and the analytically known Fourier kernels.

Interpolation is yet another way of overcoming the difficulty of having partial knowledge on the original signal. In such an approach, the signal is assumed to lie within a predefined shift-invariant space. In some spaces the original continuous-domain signal can be fully reconstructed from its ideal samples [4], [5] and its representation coefficients can be exactly calculated. This property is useful in LTI systems where the input signal is projected onto a shift-invariant space defined by the impulse response function. Within this setup the ideal samples of the output signal can be utilized to reconstruct this projection [3]. However, this is not necessarily the case for finite-support signals and images, for which an alternative approach to approximating representation coefficients is required.

Discrete-domain data can also be manipulated by a digital filter. Current filter design methods rely on frequency domain characteristics, e.g., identifying the pass- and stop-band frequencies and determine tolerance parameters and filter order [6]. Within the context of continuous vs. discrete signal processing, a digital filter should approximate the continuous-domain output signal rather than the frequency response of the analog filter alone; it is not guaranteed that similar frequency characteristics would yield similar output signals. By analyzing the overall effect induced by the sampling process, an alternative design scheme may be derived.

Inverse problems are of interest as well. A blurred image is the result of convolving the original continuous-space image with a certain kernel. The ensued discrete version corresponds then to the sampled version of the output signal. Similar to the digital filter design situation, this sampled version can be processed to approximate the sampled version of the original image itself. This alternative deconvolution approach should consider the nature of the sampling process as well as the continuous-domain convolution operation.

Another continuous vs. discrete issue is concerned with differential operators. Numerically solving differential equations involves discretization. For instance, a common way for approximating the continuous-domain derivative is the backward (forward) difference method. Here also, the discrete approximation scheme does not take the sampling process into account and an alternative scheme may be required instead. This observation is also relevant to the direct implementation of differential operators commonly used in image processing algorithms [7].

This work is motivated by image processing applications for which combined space representation schemes have been widely used. For instance, the Gabor, wavelet and contourlet transforms were found to be adequate for obtaining a sparse representation [8]–[11]. Sparsification in turn was shown to be useful for super resolution algorithms, blind source separation and deconvolution, as well as for entropy-based image compression applications to name a few [12]–[17]. Combined space representation schemes are also adopted for feature extraction and similarity assessments [8], [18], [19]. Also, the DFT, DCT and other related transforms such as the polar Fourier transform [20] play an important role in image processing algorithms as do partial differential equations [7], [21], [22].

The common denominator of all these algebraic operations is the inner product. The key point here is that any linear bounded functional in a certain Hilbert space can be described by means of an inner product due to Riesz representation theorem [23]. The main goal of this paper is to investigate the effect of the sampling process on such functionals within the context of images. In particular, suggesting alternative image processing schemes that utilize the properties of the sampling scheme (ideal and non-ideal, uniform and non-uniform) while considering a robust minimax approximation approach. A similar approach was considered in [24] for the infinite support signals. This work extends and generalizes those results to finite-support signals and images, giving rise to more practical applications.

The paper is organized as follows. We begin with mathematical preliminaries, then describe the ideal sampling process by means of set transforms while focusing on finite support signals. We consider generalized (non-ideal) sampling and further show that the one-dimensional scheme is naturally adopted to images. In Section IV we establish intertwining relations of inner products defined over several Hilbert spaces. In particular, we state some results connecting $L_2(\Omega)$, ℓ_2 and Sobolev inner products. We then show that the derivative calculation and the Fourier transform evaluation can be described by means of a set transform as well. In Section V we present a minimax approximation scheme and analyze its properties. Potential applications such as approximating the Fourier transform or the derivative operation, as well as approximating the output of an LTI system are discussed in detail. 2D examples are given in Section VI followed by conclusions in Section VII.

II. Mathematical Preliminaries

Let $\mathcal{H}$ be a Hilbert space and let $\{s_n\} \in \mathcal{H}$ be a frame for

$$\mathcal{S} = Span\,\{s_n(t)\} \subseteq \mathcal{H}. \tag{1}$$

Then, the set transform S is given by

$$\begin{aligned} &S : \ell_2 \to \mathcal{S} \\ &Sc = \sum_{n=0}^{N-1} c_n \cdot s_n, \end{aligned} \tag{2}$$

with its adjoint being

$$\begin{aligned} &S^* : \mathcal{H} \to \ell_2 \\ &S^* x = \sum_{n=0}^{N-1} \langle x, s_n \rangle_{\mathcal{H}} \cdot e_n. \end{aligned} \tag{3}$$

The set $\{e_n\}$ denotes the standard basis of ℓ_2. An orthogonal projection onto a closed subspace $\mathcal{A}$ is denoted by $P_{\mathcal{A}}$ and the space $\mathcal{A}^{\perp}$ is the orthogonal complement of $\mathcal{A}$ in $\mathcal{H}$. The Moore-Penrose pseudo inverse of a bounded transformation is denoted by a † superscript. An open interval on the real line or on the real plane is denoted by Ω. We will assume with no loss of generality that $\Omega = (-\pi, \pi)$ or $\Omega = (-\pi, \pi) \times (-\pi, \pi)$ for the one-dimensional case or for images, respectively. $H_2^p(\Omega)$ denotes the Sobolev space of order p [25]. This special Hilbert space consists of all functions satisfying $x, x^{(1)}, \ldots x^{(p)} \in L_2(\Omega)$ where $x^{(p)}$ is the *p*-th derivative of x. The corresponding inner product is

$$\langle x, y \rangle_{H_2^p(\Omega)} = \sum_{n=0}^{p} \int_{\Omega} x^{(n)}(t) \cdot \overline{y^{(n)}(t)}\, dt. \tag{4}$$

Alternatively, one can express this inner product within the frequency domain:

$$\langle x, y \rangle_{H_2^p(\Omega)} = \frac{1}{2\pi} \int_{-\infty}^{\infty} X(\omega)\, \overline{Y}(\omega) \cdot (1 + \omega^2 + \cdots + \omega^{2p})\, d\omega. \tag{5}$$

The Fourier transform operator (continuous or discrete) is denoted by $\mathcal{F}$ and convolution is denoted by $*$.

III. IDEAL SAMPLING AS A SET TRANSFORM

We consider first the ideal sampling scheme and interpret it as an orthogonal projection within a Sobolev space. This restriction to Sobolev rather than to $L_2(\Omega)$ spaces is two-fold: recalling the standard $L_2(\Omega)$ norm, identical functions might yield different sampling sequence giving rise to a one-to-many mapping; also, the distinct sampling points have a Lebesgue measure of zero thus introducing a non-bounded transformation.

The infinite-support case was recently investigated in [24] and in [26]. It was shown there that the ideal sampling process can be described by means of a proper set transform. Specifically, the sampled value of a continuous-time signal $x \in H_2(\Omega)$ can be described by the inner-product operation

$$x(t_0) = \langle x, s_n \rangle_{H_2(\Omega)}\,, \tag{6}$$

where $s_n(t) = e^{-|t-t_0|}/2$. In the current work we extend this result and characterize the appropriate sampling function for the finite-support case.

A. Finite-support signals

Consider Sobolev signals having a finite open support Ω. The following lemma enables one to interpret the ideal sampling process by means of inner product calculations in a Sobolev space. The importance of this result will be evident later on, when continuous-domain operations will be approximated by sampled data.

Lemma 1: Let $x \in H_2(\Omega)$ where $\Omega = (-\pi, \pi)$. Given $t_0 \in \Omega$, the sampled value $x(t_0)$ is given by

$$x(t_0) = \langle x, s_{t_0} \rangle_{H_2(\Omega)}\,, \tag{7}$$

where

$$\begin{cases} s(t) &= \frac{1}{2\pi}\sum_n \frac{1}{1+n^2} \cdot e^{jnt}. \\ s_{t_0}(t) &= s(t-t_0). \end{cases} \tag{8}$$

Proof: x is a Sobolev function having a finite support and can be expressed by means of a Fourier series

$$x(t) = \sum_n a_n \cdot e^{jnt}, \tag{9}$$

where $a \in \ell_2$. In particular, for any $t_0 \in \Omega$ the equation

$$x(t_0) = \sum_n a_n \cdot e^{jnt_0}, \tag{10}$$

holds point wise. The sampled value of x is a linear bounded functional and by Riesz representation theorem can be described by means of an inner product

$$x(t_0) = \langle x, s_{t_0} \rangle_{H_2(\Omega)}, \tag{11}$$

where $s_{t_0} \in H_2(\Omega)$ is unique. Let s_{t_0} be described by the Fourier coefficients $b \in \ell_2$. Then, the latter equation yields

$$\begin{aligned} \sum_n a_n \cdot e^{jnt_0} &= \int_\Omega x \cdot \overline{s}_{t_0}\, dt + \int_\Omega x' \cdot \overline{s'}_{t_0}\, dt \\ &= \sum_{n,m} a_n \overline{b}_m (1 + n \cdot m) \int_\Omega e^{j(n-m)t}\, dt \\ &= 2\pi \sum_n a_n \overline{b}_n (1 + n^2), \end{aligned} \tag{12}$$

where the equation holds for any $a \in \ell_2$. It follows then that

$$b_n = \frac{1}{2\pi} \cdot \frac{1}{1+n^2} \cdot e^{-jnt_0}. \tag{13}$$

$\square$

This sampling function is Ω-periodic (Figure 1). Given a set of sampling points $\{t_n\}$, the corresponding sampling functions $\{s_n(t)\} \in H_2(\Omega)$ give rise to a set transform S.

Corollary 1: If the sampling functions constitute a frame for $\mathcal{S} \in H_2(\Omega)$, then S corresponds to an orthogonal projection onto $\mathcal{S}$. Namely, $P_{\mathcal{S}} x = S(S^* S)^{\dagger} c$ where $c = S^* x$ are the ideal samples of x.

It is noted that the frame condition is met whenever the number of sampling points is finite as is the case in image processing applications. Also, no restrictions are made as for the sampling grid itself (uniform or non-uniform).

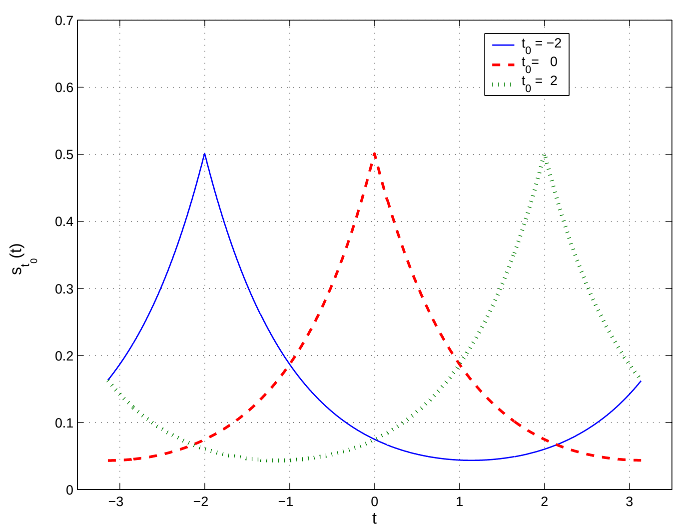

Fig. 1. Given t_0, the sampling function s_{t_0} satisfies $x(t_0) = \langle x, s_{t_0} \rangle_{H_2(\Omega)}$. Shown are sampling functions for $t_0 = -2, 0, 2$ where $\Omega = (-\pi, \pi)$.

This interpretation of the ideal sampling scheme as an orthogonal projection in a certain Hilbert space is significant in the sense of uniting the continuous-domain signal with the discrete-domain. In this regard, the Sobolev functions are dense in $L_2(\Omega)$. Thus, restricting the ideal sampling operator to such functions still maintains generality of the results. It is also noted that non-uniform ideal sampling is adequately described by this formulation and the frame condition for such a scheme remains a necessary condition for synthesizing $P_{\mathcal{S}}x$.

B. Generalized sampling

Sampling by non-ideal acquisition devices has also been put into the context of set transforms [2], [27]–[32]. That is, the sample sequence is the result of consecutive $L_2(\Omega)$ inner products where the sampling functions are known a priori. It is shown here that such $L_2(\Omega)$ sampling schemes can alternatively be described by means of Sobolev inner products. As in the infinite case [26], this description will be found useful for solving approximation problems while imposing a smoothness constraint on the original continuous-domain signal. Let $\{s_n(t)\}$ be a set of sampling functions in $L_2(\Omega)$ constituting a frame for their span. The generalized samples of $x \in L_2(\Omega)$ are then given by

$$c[n] = \langle x, s_n \rangle_{L_2(\Omega)} . \tag{14}$$

Assuming that $x \in H_2(\Omega)$, a proper description of the sampling process would then be $c[n] = \langle x, \hat{s}_n \rangle_{H_2(\Omega)}$, where $\hat{s}_n \in H_2(\Omega)$ is dependent on $s_n \in L_2(\Omega)$ and on Ω. In particular (see Section IV-A)

$$\hat{s}_n(t) = s_n(t) * \frac{1}{2\pi} \sum_n \frac{1}{1+n^2} \cdot e^{jnt}, \tag{15}$$

where the convolution operation is cyclic. These Sobolev sampling functions give rise to a set transform $\widehat{S} : \ell_2 \to \widehat{\mathcal{S}}$ where $\widehat{\mathcal{S}} \in H_2(\Omega)$. However, it is not guaranteed that the frame condition is still met in $H_2(\Omega)$. In fact, it can be proved that while the upper frame bound of $\{s_n\}$ in $L_2(\Omega)$ is a suitable choice for $\{\hat{s}_n\}$ in $H_2(\Omega)$, the lower frame bound might equal zero [33]. This zero bound, in turn, does not allow the reconstruction of $P_{\widehat{\mathcal{S}}}x$ in $H_2(\Omega)$ [34].

C. Extension to images

The one-dimensional Sobolev space extends to the two-dimensional case in the following manner. Let $\alpha = (\alpha_1, \alpha_2)$ be a tuple of nonnegative integers where $|\alpha| = \alpha_1 + \alpha_2$. Also, let

$$D^\alpha = \frac{\partial^{\alpha_1}}{\partial \zeta_1} \cdot \frac{\partial^{\alpha_2}}{\partial \zeta_2}. \tag{16}$$

We consider a two-dimensional Sobolev space of order $p \geq 1$ defined over a finite open support $\Omega = (-\pi, \pi) \times (-\pi, \pi)$. This space consists of functions $x(\zeta_1, \zeta_2)$ that satisfy $D^\alpha x \in L_2(\Omega)$ for all possible α satisfying $|\alpha| \leq p$.

The corresponding inner product is given by [25]

$$\langle x,y\rangle_{H_2^p(\Omega)} = \sum_{\{\alpha:\, 0\leq|\alpha|\leq p\}} \langle D^\alpha x, D^\alpha x\rangle_{L_2(\Omega)}. \tag{17}$$

For example, the inner product of $H_2(\Omega)$ (i.e. $p=1$) is given by

$$\langle x,y\rangle_{H_2(\Omega)} = \langle x,y\rangle_{L_2(\Omega)} + \left\langle \frac{\partial x}{\partial \zeta_1}, \frac{\partial y}{\partial \zeta_1}\right\rangle_{L_2(\Omega)} + \left\langle \frac{\partial x}{\partial \zeta_2}, \frac{\partial y}{\partial \zeta_2}\right\rangle_{L_2(\Omega)}.$$

It follows that the sampling function for such a case is given by

$$s(\zeta_{1,0},\zeta_{2,0};\zeta_1,\zeta_2) = \frac{1}{4\pi^2}\sum_{n,m}\frac{1}{1+n^2+m^2}\cdot e^{jn(\zeta_1-\zeta_{1,0})}\cdot e^{jm(\zeta_2-\zeta_{2,0})},$$

where $(\zeta_{1,0},\zeta_{2,0})$ is the sampling point. It is pointed out that this sampling function (Figure 2) cannot be separated into a multiplication of two one-dimensional functions. Also, there is no restriction on the sampling grid. If the sampling functions constitute a frame for their span, then $P_{\mathcal{S}}x$ can be analytically synthesized. This latter requirement is met whenever the number of samples is finite. Also, motivated by [35], it is noted that different sampling schemes, such as ideal and non-ideal schemes, can be incorporated into a single unifying set transform.

D. Extension to Sobolev spaces of higher orders

The sampling function of Lemma 1 considers Sobolev functions of order $p=1$. Nevertheless, for some applications the continuous-domain model is known a priori to consist of smoother functions. This model corresponds to Sobolev functions of order $p\geq 1$. Considering such cases, the sampling function for the one-dimensinal case satisfies

$$s(t) = \frac{1}{2\pi}\sum_{n}\frac{1}{1+n^2+\cdots+n^{2p}}\cdot e^{jnt}, \tag{18}$$

where

$$\lim_{p\to\infty} s(t) = \frac{1}{2\pi}. \tag{19}$$

Figure 3 depicts sampling functions for several orders.

IV. Intertwining Relations of Inner Products

The $L_2(\Omega)$ inner product plays a key role in combined spaces representation for both one-dimensional signals and images [8], [10], [11], [18], [36]–[42]. It is shown here that such inner products can be expressed by means of Sobolev inner products. Also, Sobolev inner products are shown to be adequate for describing the derivative and the Fourier transform operations.

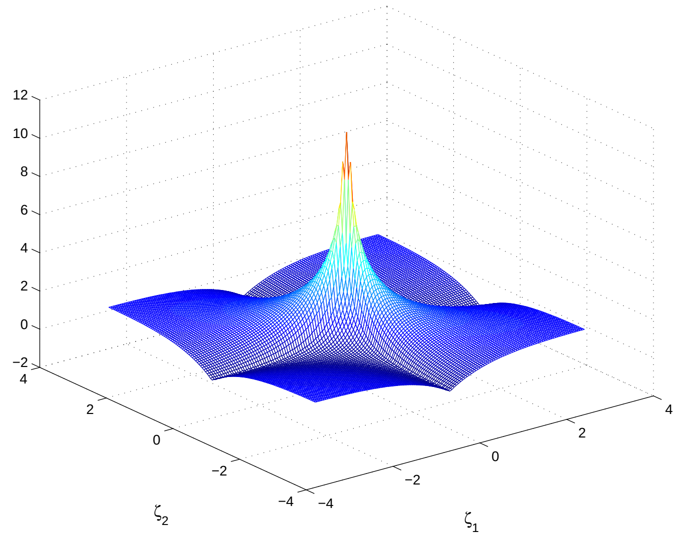

(a)

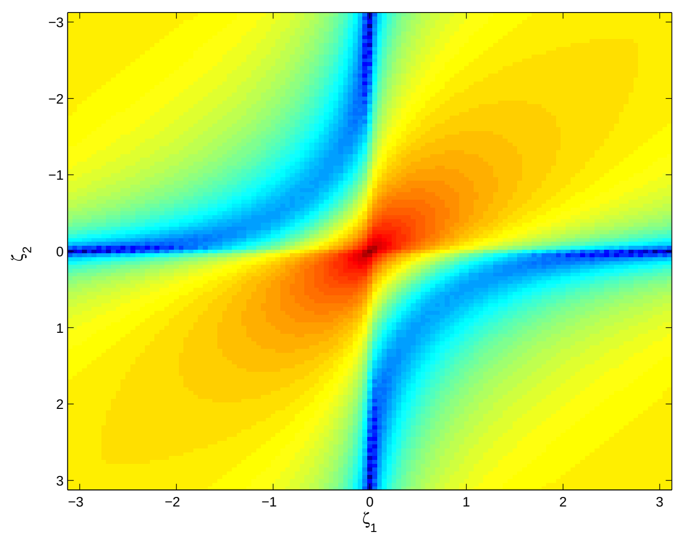

(b)

Fig. 2. Given $(\zeta_{1,0}, \zeta_{2,0})$, the two-dimensional sampling function $s(\zeta_{1,0}, \zeta_{2,0}; \zeta_1, \zeta_2)$ satisfies $x(\zeta_{1,0}, \zeta_{2,0}) = \langle x, s \rangle_{H_2(\Omega)}$. Shown is the function itself (a) and the image of its logarithm (b) for $(\zeta_{1,0}, \zeta_{2,0}) = (0, 0)$.

A. L_2, ℓ_2 and Sobolev inner products

The following lemma establishes an intertwining relationship between $L_2(\Omega)$ and $H_2(\Omega)$ inner products.

Lemma 2: Let $y \in L_2(\Omega)$. Then, $\forall x \in H_2(\Omega)$

$$\langle x, y \rangle_{L_2(\Omega)} = \langle x, y * s \rangle_{H_2(\Omega)}, \tag{20}$$

where $y * s$ is a continuous-domain periodic convolution and s is given in Lemma 1.

Proof: Let $I : H_2(\Omega) \to L_2(\Omega), Ix = x$. This operator is bounded and has an adjoint. Given $y \in L_2(\Omega)$, the equation

$$\langle x, y \rangle_{L_2(\Omega)} = \langle x, I^* y \rangle_{H_2(\Omega)} \tag{21}$$

holds for any $x \in H_2(\Omega)$. Let $a, b, c \in \ell_2$ be the Fourier coefficients of x, y and I^*y, respectively. Then, the equality

$$2\pi \sum_n a_n \overline{b}_n = 2\pi \sum_n a_n \overline{c}_n \cdot (1 + n^2) \tag{22}$$

holds for any a, yielding $c_n = b_n / 1 + n^2$. This relation can then be shown to coincide with the continuous-domain periodic convolution $y * s$. $\square$

This intertwining relationship between inner products enables one to interpret any $L_2(\Omega)$ linear bounded functional by means of an $H_2(\Omega)$ functional. Recalling that the ideal sampling process was shown to coincide with a proper set transform in $H_2(\Omega)$, we have established a framework connecting continuous-domain operations with discrete-domain calculations. This connection is further investigated in Section V where approximation issues are addressed.

Another type of intertwining relation considers the ℓ_2 inner product as reflected by the adjoint of the sampling set transform. Let $x \in \mathcal{H}$, and let $c = S^*x$ be its sampled version. Here $S : \ell_2 \to \mathcal{S} \subseteq \mathcal{H}$ is a set transform describing the sampling process (ideal or non-ideal). Then, $\forall a \in \ell_2$ $\langle c, a \rangle_{\ell_2} = \langle x, Sa \rangle_{\mathcal{H}}$. Furthermore, by setting a to be the sampled version of an arbitrary analysis function, the ℓ_2 inner product resembles a Riemann type sum. As a result, the equivalence of this inner product with the inner product of $\mathcal{H}$ provides a quantitative measure for comparing the Riemann type sum approximation scheme with any other scheme, in particular with the minimax scheme. This issue is addressed in Section V too.

B. Derivative evaluation

We focus on calculating the derivative of a signal at a countable set of points. In particular, we wish to describe the ideal uniform sampled version of the derivative by means of a set transform. For introducing a well posed problem, one must guarantee that this sampled version would be a member of ℓ_2. Thus, we restrict the admissible

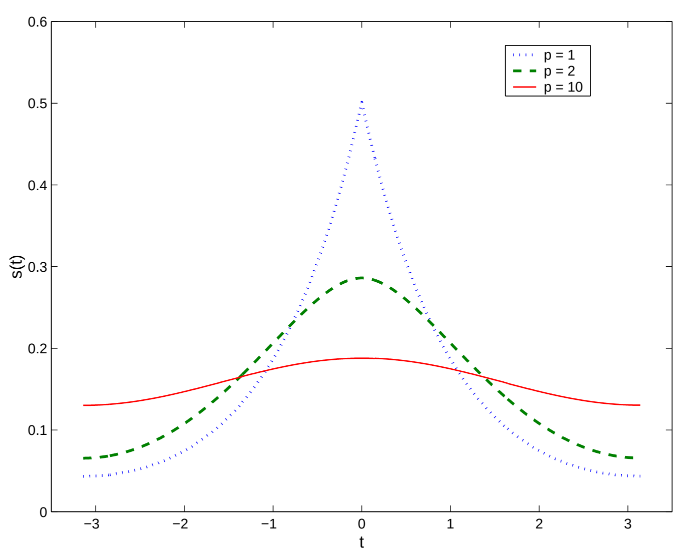

Fig. 3. Similar to Figure 1. Shown are sampling functions corresponding to several Sobolev orders $p = 1, 2, 10$. Here $\Omega = (-\pi, \pi)$.

signals to be Sobolev functions of order $p = 2$. The following lemma introduces a new way to calculate the derivative value of a Sobolev signal at a given point.

Lemma 3: Let $x \in H_2^p(\Omega)$ where $p = 2$, $\Omega = (-\pi, \pi)$, and let $t_0 \in \Omega$. Then, $x^{(1)}(t_0)$ is given by

$$x^{(1)}(t_0) = \langle x, w_{t_0} \rangle_{H_2(\Omega)}, \tag{23}$$

where

$$w_{t_0}(t) = \frac{1}{2\pi j} \sum_n \frac{n}{1 + n^2 + n^4} \cdot e^{jn(t-t_0)}, \ t \in \Omega. \tag{24}$$

Proof: Let $x = \sum_n a_n \cdot e^{jnt}$, $a \in \ell_2$, where equality holds point-wise. The sampled value of $x^{(1)}$ is then given by

$$x^{(1)}(t_0) = \sum_n jn \cdot a_n \cdot e^{jnt_0}. \tag{25}$$

The proof then is similar to the proof of Lemma 1 while utilizing the appropriate Sobolev inner product for $p = 2$.

□

The set transform interpretation arises then from evaluating the derivative function at a countable set of points. Practically, using digital means, this last result can be used for calculating the derivative function of a signal. Similar derivations extend this formulation to images as was done in Section III-C. Also, this formulation can be naturally adopted when extracting values of higher derivative orders. Figure 4 depicts $w_{t_0}(t)$ for the finite-support case for several sampling points. It is also noted here that this differentiating functional resembles other differentiation masks that are used for edge detection in image processing applications [43], [44], and in this regard this very function (24) provides the exact masking function to be approximated, as shown in Section V.

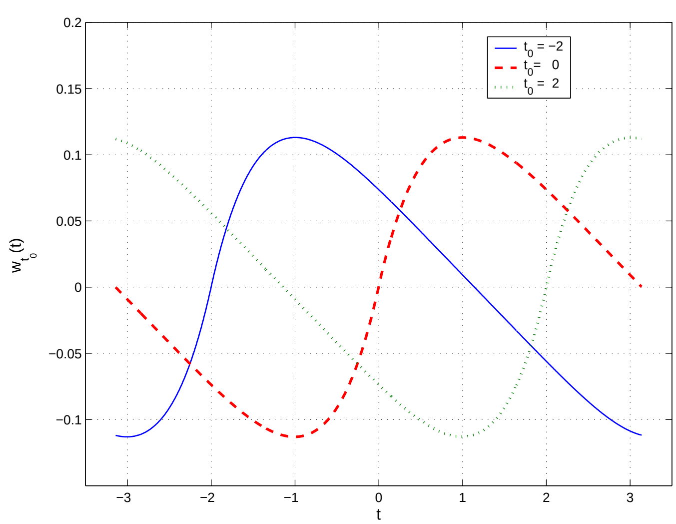

Fig. 4. Given t_0, the analysis function w_{t_0} satisfies $x^{(1)}(t_0) = \langle x, w_{t_0} \rangle_{H_2^p(\Omega)}$. Shown are the analysis functions for $t_0 = -2, 0, 2$. The order of the Sobolev space is $p = 2$ and $\Omega = (-\pi, \pi)$.

C. Fourier transform evaluation

We focus on describing Fourier transform values by means of a set transform. Alternatively, we find an analysis function $w_{\omega_0}(t) \in \mathcal{H}$ for which $X(\omega_0) = \langle x, w_{\omega_0} \rangle_{\mathcal{H}}$. It so happens that such a description is not possible for $L_2(\Omega)$ space in the case of $\Omega = \mathbb{R}$. This is due to the fact that $X(\omega_0)$ is not a bounded functional; one may consider a scaled and normalized version of the $sinc(\cdot)$ function and observe that the DC component $X(\omega = 0)$ may be arbitrarily large although the $L_2(\Omega)$ norm is maintained fixed. Nevertheless, finite support signals are adequate for a bounded set transform description.

First, recall that the Fourier transform of $x \in L_2(\Omega)$ is given by

$$X(\omega) = \int_{\Omega} x(t) \cdot e^{-j\omega t} \, dt. \tag{26}$$

Here $\Omega = (-\pi, \pi)$. A sample value of the Fourier transform has an inner product interpretation given by

$$X(\omega_0) = \left\langle x(t), e^{j\omega_0 t} \right\rangle_{L_2(\Omega)}. \tag{27}$$

Following Lemma 2, this $L_2(\Omega)$ inner product can be represented by means of a Sobolev inner product. The following lemma describes the Fourier transform value of a signal at an arbitrary frequency by means of a Sobolev inner product.

Lemma 4: Let $x \in H_2(\Omega)$ where $\Omega = (-\pi, \pi)$, and let $X(\omega_0)$ be the value of its Fourier transform at an arbitrary frequency ω_0. Then,

$$X(\omega_0) = \langle x, w_{\omega_0} \rangle_{H_2(\Omega)}, \tag{28}$$

where

$$w_{\omega_0}(t) = \sum_n \frac{1}{1+n^2} \cdot \frac{sin\left[\pi(\omega_0 - n)\right]}{\pi(\omega_0 - n)} \cdot e^{jnt}. \tag{29}$$

Proof: This result stems from Lemma 2. □

Note that the analysis function (29) reduces to a single harmonic when $\omega_0 \in \mathbb{Z}$. Figure 5 depicts the real and imaginary parts of $w_{\omega_0}(t)$ for $\omega_0 = 10.5, 80.5$. The set transform characterization arises from evaluating the Fourier transform at a countable set of frequencies.

V. Minimax Approximation

This description in a Sobolev space of the sampling process and of linear functionals allows for a minimax approximation scheme based on the sampled version of a signal. Both ideal and non-ideal sampling schemes are naturally considered. This minimax approach provides an alternative approximation scheme to currently available methods such as the Riemann type sum and other interpolation algorithms. For instance, the discrete Fourier

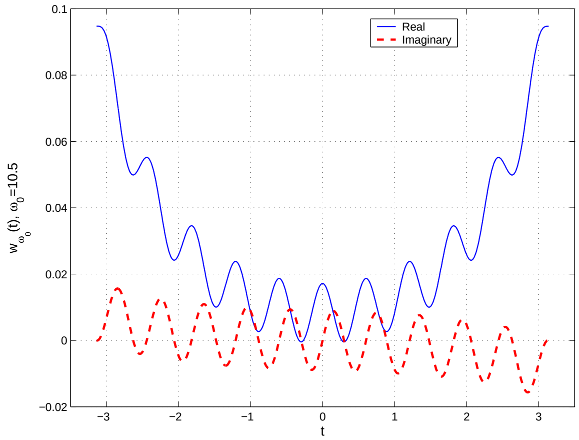

(a)

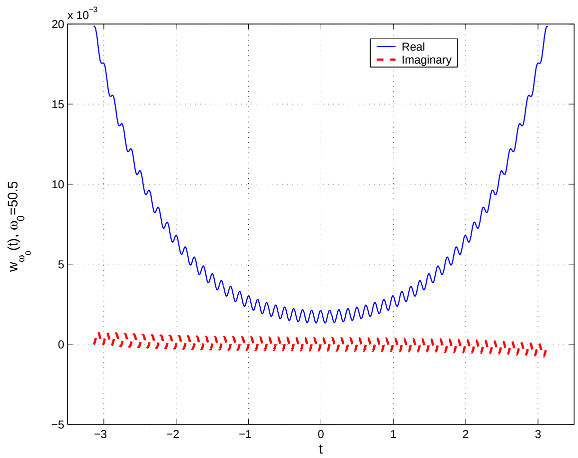

(b)

Fig. 5. Given ω_0, the analysis function w_{ω_0} satisfy $X(\omega_0) = \langle x, w_{\omega_0} \rangle_{H_2(\Omega)}$. Here $X(\omega)$ is the Fourier transform of $x \in H_2(\Omega)$. Shown are the real (solid) and imaginary (dashed) parts of the analysis function for $\omega_0 = 10.5$ (a) and 50.5 (b).

transform (DFT) provides a Riemann type approximation of the Fourier transform of a continuous-domain signal. Nevertheless, we show here that a superior minimax approach could be used instead.

Let $\mathcal{H}$ be a Hilbert space and let W be a set transform corresponding to a set of analysis functions $\{w_n\}$. It is assumed that this set of functions constitutes a frame for its span $\mathcal{W} \subseteq \mathcal{H}$. The result of analyzing a signal $x \in \mathcal{H}$ is denoted by the ℓ_2 sequence $d = W^*x$. The question raised then concerns the best possible approximation scheme for d while having the samples of the original continuous-domain signal as the only available data. We consider a minimax criterion for approximating the sequence d while using the ℓ_2 standard metric. This problem was recently addressed in [26]. Let $c = S^*x$ be the known samples of $x \in \mathcal{H}$. Then, the solution of

$$\arg\min_{\hat{d}} \max_{c, \|x\|_{\mathcal{H}} \leq L} \left\| d - \hat{d} \right\|_{\ell_2} \tag{30}$$

is given by

$$\hat{d} = W^* S (S^* S)^{\dagger} c. \tag{31}$$

This minimax solution corresponds to analyzing the orthogonal projection of x onto $\mathcal{S}$, namely $\hat{d} = W^* P_{\mathcal{S}} x$. Also, this solution is element-wise optimal. Approximating $d[n]$ depends on the single analysis function w_n alone (Figure 6). Alternatively, the minimax solution is optimal in any ℓ_p sense ($p = 1, 2, \ldots$).

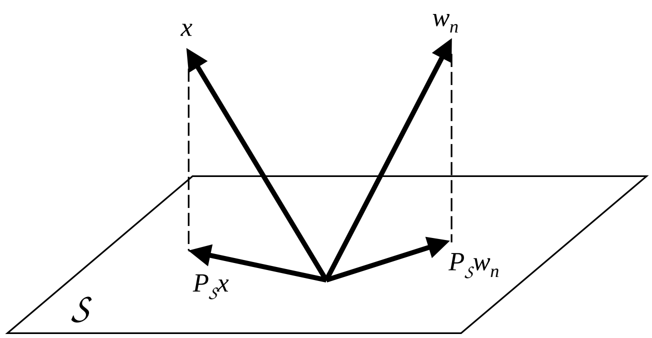

Fig. 6. Vector interpretation for the minimax solution. Here $d[n] = \langle x, w_n \rangle$ is approximated by $\hat{d}_n = \langle P_{\mathcal{S}} x, P_{\mathcal{S}} w_n \rangle$.

It can be shown that if the original signal is a Sobolev function, the minimax solution for such a case corresponds to a proper oblique projection [26]. Although the solutions are different, both are independent of the constant L. However, this upper bound determines the approximation error. It holds that

$$x = P_{\mathcal{S}} x + P_{\mathcal{S}^\perp} x, \tag{32}$$

where $P_{\mathcal{S}} x$ is analytically known. It then follows that

$$\|P_{\mathcal{S}^\perp} x\|_{\mathcal{H}} = \sqrt{L^2 - \|P_{\mathcal{S}} x\|_{\mathcal{H}}^2}. \tag{33}$$

This last expression implies that even though L is arbitrarily chosen, it must satisfy $L \geq \|P_{\mathcal{S}} x\|$. We wish to identify the worst case signal that would yield the maximum possible approximation error given by

$$e_m = \left\| d - \hat{d} \right\|_{\ell_2} = \|W^* P_{\mathcal{S}^\perp} x\|_{\ell_2}. \tag{34}$$

Clearly this worst case signal satisfies (32). Thus it remains to identify the exact expression for $P_{\mathcal{S}^\perp} x$ that yields the maximum possible approximation error e_m. We recall the property of a Bessel sequence [45]

$$\sum_n \left| \langle x, y_n \rangle_{H_2(\Omega)} \right|^2 \leq B \cdot \|x\|_{H_2(\Omega)}^2, \tag{35}$$

and state the following result.

Theorem 1: Let $\hat{d} \in \ell_2$ satisfy (31), and let $\{P_{\mathcal{S}^\perp} w_n\}$ be a Bessel sequence for its span. Then,

$$e_m^2 \leq B \cdot \left(L^2 - \|P_{\mathcal{S}} x\|_{\mathcal{H}}^2 \right), \tag{36}$$

where B is the corresponding Bessel bound.

Proof: Notice that $e_m[n] = \langle P_{\mathcal{S}^\perp} w_n, P_{\mathcal{S}^\perp} x\rangle$. Applying the Bessel bound

$$\begin{aligned}\left\|d-\hat{d}\right\|_{\ell_2}^2 &= \|W^* P_{\mathcal{S}^\perp} x\|_{\ell_2} \\ &= \sum_n |\langle P_{\mathcal{S}^\perp} x, P_{\mathcal{S}^\perp} w_n\rangle|^2 \\ &\leq B\cdot \|P_{\mathcal{S}^\perp} x\| \\ &\leq B\cdot\left(L^2 - \|P_{\mathcal{S}} x\|_{\mathcal{H}}^2\right). \end{aligned} \tag{37}$$

□

If $\{P_{\mathcal{S}^\perp} w_n\}$ is a finite set of linearly independent functions, then B is equal to the maximum eigenvalue of their corresponding Gram matrix. If this set is not a Bessel sequence then the approximation error can be made arbitrarily large.

The minimax solution of (31) can be compared with the Riemann type sum method [26]. For example, let $c = S^* x$ be the ideal uniform samples of $x \in H_2(\Omega)$ and let $b = S^* w$ be the samples of a single analysis function $w \in L_2(\Omega)$ (assuming that $b \in \ell_2$). Then, the Riemann sum approximation is given by

$$T\sum_n c[n]\cdot \overline{b[n]} = \langle P_{\mathcal{S}} x, T\cdot Sb\rangle_{H_2(\Omega)}. \tag{38}$$

Denoting e_r to be the Riemann sum approximation error, it follows that

$$\begin{aligned} e_r^2 &= |\langle P_{\mathcal{S}^\perp} x, P_{\mathcal{S}^\perp}\hat{w}\rangle + \langle P_{\mathcal{S}} x, P_{\mathcal{S}}\hat{w} - T\cdot Sb\rangle| \qquad (39)\\ &\leq \|P_{\mathcal{S}^\perp} x\|\cdot\|P_{\mathcal{S}^\perp} w\| + \|P_{\mathcal{S}} x\|\cdot\|P_{\mathcal{S}}\hat{w} - T\cdot Sb\|, \end{aligned}$$

where all inner products and norms are in $H_2(\Omega)$ and $\hat{w} = w * s$. The sampling function s is given by Lemma 1. Finally,

$$\max e_r^2 = \max e_m^2 + C, \tag{40}$$

where $C = \|P_{\mathcal{S}} x\|\cdot\|P_{\mathcal{S}}\hat{w} - T\cdot Sb\|$ is a known constant, providing a measure of comparison between the Riemann type sum and the minimax approximation schemes. It is noted here that the element-wise property of the minimax solution still holds for $\left|\max e_r^2 - \max e_m^2\right|$, and comparing the two approximation schemes is also possible when introducing several analysis functions.

Having established a minimax solution and analyzed its performance, it is now possible to apply this approximation scheme to an arbitrary linear bounded functional as given by the next theorem.

Theorem 2: Let $x \in H_2(\Omega)$ be known by its ideal samples $c \in \mathbb{C}^N$ and let $d = \langle x, w\rangle$ be a linear bounded functional described by $w \in H_2(\Omega)$. Then, the minimax approximation of d is given by

$$\hat{d} = c \cdot G_s^{-1} \cdot q^T, \tag{41}$$

where

$$G_s[m,n] = \langle s_m, s_n \rangle_{H_2(\Omega)} \tag{42}$$

is the Gram matrix of the proper sampling functions $\{s_n\}$ (as in Lemma 1) and $q \in \mathbb{C}^N$ are the ideal samples of w.

Proof: The finite set of sampling functions $\{s_n\}$ are linearly independent and have a biorthogonal set. The sequence c corresponds to the representation coefficients of $P_{\mathcal{S}}x$ by this biorthogonal set, whereas $G_s^{-1} \cdot q^T$ corresponds to the representation coefficients of $P_{\mathcal{S}}w$ by the sampling functions themselves. Following the minimax solution of (31)

$$\hat{d} \quad = \quad \langle P_{\mathcal{S}}x, w \rangle_{H_2(\Omega)} = c \cdot G_s^{-1} \cdot q^T.$$

□

This theorem could be useful for numerical implementation. Having the sampled version of a signal, it states that any linear bounded functional can be approximated by matrix calculations. No continuous-domain operations are further required. Possible applications include the calculation of representation coefficients, the approximation of Fourier transform values and the approximation of the derivative values. The main task is to identify the proper analysis functions to be applied. We are focusing on two possible applications. The first is a minimax scheme for approximating the Fourier transform value at a finite set of frequencies. The second application addresses the problem of approximating sampled values of the output of an LTI (1D) or an LSI (2D) system.

A. Fourier transform

We assume that $x \in H_2(\Omega)$, where $\Omega = (-\pi, \pi)$. The uniform ideal sampling scheme is given by $c = S^* x$. In particular,

$$\begin{aligned} S \quad &: \quad \mathbb{C}^N \to \mathcal{S} \subseteq H_2(\Omega) \\ Sc \quad &= \quad \sum_{n=-\frac{N-1}{2}}^{\frac{N-1}{2}} c\,[n] \cdot s(t - nT). \end{aligned} \tag{43}$$

Here N corresponds to the number of available samples, assumed to be an odd number. $s(t)$ is given by Lemma 1. Having this sampled version of a signal, it is a common practice to apply a DFT for approximating the Fourier transform of the original signal:

$$X^{D}[k]=\sum_{n=-\frac{N-1}{2}}^{\frac{N-1}{2}}c[n]\cdot e^{-j\frac{2\pi nk}{N}}. \tag{44}$$

The N values of the DFT serve then as a Riemann type sum approximation of the Fourier transform (up to multiplication by T) at equally spaced frequencies

$$\omega_k=\frac{2\pi}{NT}k,\;\;|k|\leq\frac{N-1}{2}. \tag{45}$$

This approximation is by no means optimal in the minimax sense; utilizing the proposed minimax solution one can apply the following corollary.

Corollary 2: The minimax approximation of $d=X(\omega_0)$ is given by the sampled version of (29).

This corollary together with Theorem 2 provides an alternative method, other than the DFT, for approximating sampled values of the Fourier transform of a continuous-domain signal. It extends naturally to images and can be adopted for other image-related transforms as well [**?**], [20], [44], [46]. The derivative functional is applicable as well.

Corollary 3: The minimax approximation for $d=x^{(1)}(t_0)$ is given by the sampled version of (24).

Here also, the two-dimensional case is readily extended by the formulation of Section III-C.

B. Continuous-domain filtering

Let $h(-t)\in L_2$ be the impulse response of a continuous-time LTI system and let $x\in L_2(\Omega)$ be an arbitrary input signal. Then, the sample value of the output signal at $t=t_n$ is given by

$$d\left[n\right]=\left\{x*h\right\}(t_n)=\left\langle x,h_n\right\rangle_{L_2(\Omega)}, \tag{46}$$

where $h_n(t)=h(t-t_n)$. The aim is to find a minimax approximation scheme for d. That is, approximating the sampled output of a continuous-time filter while having the sampled version of the input signal as the only available data.

Let $\mathcal{S}\subset L_2(\Omega)$ (i.e., $\Omega=\mathbb{R}$) be a shift-invariant space described by a shift-invariant generalized sampling scheme $S:\ell_2\to\mathcal{S}$. A minimax approximation scheme for such a case was considered in [30]. In such a setting the minimax solution $\hat{d}$ coincides with a digital filter g where $\hat{d}=c*g$. The Fourier transform of g is shown to be comprised of the autocorrelation and cross-correlation functions of the generating sampling function itself and $h(t)$. A similar expression was then derived for the uniform ideal sampling scheme too [26]. It involved an interpretation of the sampling and analysis process in a proper Sobolev space while applying the minimax scheme of (31) in this very space. Nevertheless, this digital filter interpretation does not hold for the finite-support case and another approximation scheme is required, as given by the following corollary.

Corollary 4: The minimax approximation of $d\left[n\right] = \left\{x * h\right\}\left(t_n\right)$ is given by the sampled version of

$$w_{t_n}(t) = [h(t - t_n) \cdot \chi_\Omega(t)] * s(t), \tag{47}$$

where $\chi(\Omega)$ is the characteristic function and the convolution operation is cyclic.

All of the results above can be extended to images based on Section III-C and on the definition of the open support Ω. This open support has no restrictions and the choice of $\Omega = (-\pi, \pi) \times (-\pi, \pi)$ was chosen for convenience purposes only.

VI. Examples

A. Derivative Approximation

Suppose we are given the image of Figure 7, and wish to approximate the derivative $\partial/\partial\zeta_1$ at the origin. Calculating the derivative at the origin corresponds to identifying a proper image (Figure 8) for performing a Sobolev inner product with $P_{\mathcal{S}}x$. The latter is the orthogonal projection of the original image onto the sampling space, and it is determined by all the sampled values of the image. This inner product can also be described by means of a discrete scheme utilizing the sampled version of the original image, the sampled version of Figure 8, and a proper Gram matrix (Theorem 2). Assuming ideal sampling, this Gram matrix is explicitly given by

$$G(n,m) = \frac{1}{4\pi^2} \sum_{n,m} \frac{1}{1+n^2+m^2}\, e^{jn(\zeta_{1,n}-\zeta_{1,m})} \cdot e^{jm(\zeta_{2,n}-\zeta_{2,m})},$$

where $(\zeta_{1,n}, \zeta_{2,n})$ and $(\zeta_{1,m}, \zeta_{2,m})$ are any possible pair of sampling points. Given the sampled version of the image of Figure 7, there are many continuous-space images that correspond to such a sampled version. Nevertheless, they all share the same orthogonal projection onto the sampling space (Figure 9).

B. Gradient Approximation

We utilize the minimax approach for approximating gradient values of an image given by its samples. The 2D derivative functional along the horizontal direction was shown to correspond with Figure 8. The proper Gram matrix was given in (48). Choosing a masking kernel of 3×3, one can determine the minimax kernel by applying Theorem 2

$$G^{-1} \cdot q^T = \begin{bmatrix} -\alpha & \beta & \gamma \\ -\delta & 0 & \delta \\ -\gamma & -\beta & \alpha \end{bmatrix}, \tag{48}$$

where $\alpha = 0.3\delta$, $\beta = \delta/60$ and $\gamma = 0.6\delta$.

Given an image, the gradient value at a point is given by the Pythagorean sum of the horizontal and vertical derivative values. Those values can be calculated by the standard backward difference model, or alternatively by the minimax approach presented here. Consider the image of Figure 10(a), the minimax approximation of the gradient value is given in Figure 10(b) whereas the backward difference model results in Figure 10(c). Although similar, those two figures are slightly different as evident from Figure 10(d). This difference is mainly due to different localization of the gradient value; the minimax approach approximates the derivative at the very sampling point whereas other methods do not. Another source of difference is due to different approximation values; and in this regard the minimax approach guarantees the minimization of the maximum possible error induced by the sampling process whereas other method do not.

VII. Conclusions

Sampling finite-support Sobolev signals has been shown to coincide with an orthogonal projection within proper Sobolev spaces. Since these signals are dense in $L_2(\Omega)$, restricting the input signal to belong to a Sobolev space still maintains generality of the results. Both ideal and non-ideal sampling schemes have been adopted by this interpretation. In cases where the sampling scheme is described by $L_2(\Omega)$ inner products (generalized sampling), the sampling process was expressed by yet another Sobolev inner product.

A minimax approach was then applied to approximating continuous-domain functionals while having the sampled version of the input signal as the only available data. Such linear bounded functionals can be also described by proper set transforms in a Sobolev space. Practical applications include representation coefficients approximation, Fourier transform evaluation and derivative calculations – often used in image processing applications. Such a Sobolev description for both the sampling process and the continuous-domain functionals gives rise to a closed

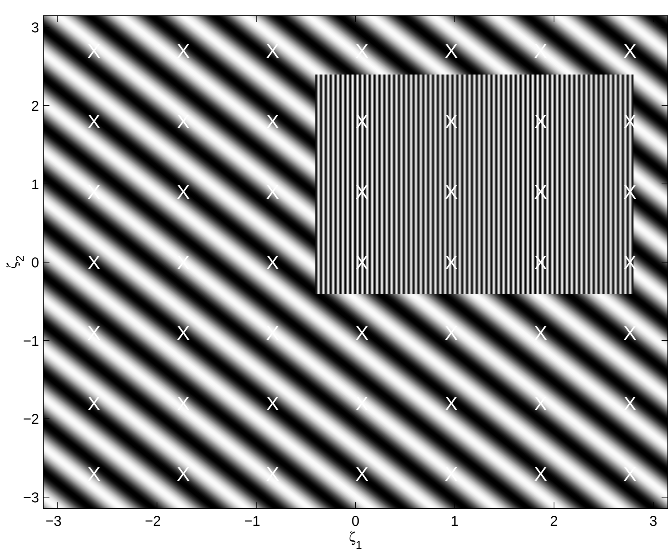

Fig. 7. A continuous-space image and a sampling grid denoted by x-marks.

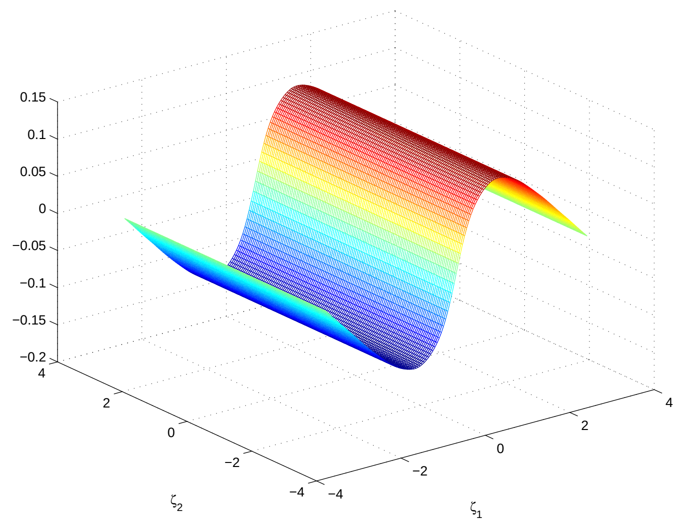

Fig. 8. A two-dimensional function that corresponds to the derivative value of a continuous-space image along the horizontal direction at the origin. The derivative value is given by a Sobolev inner product expression.

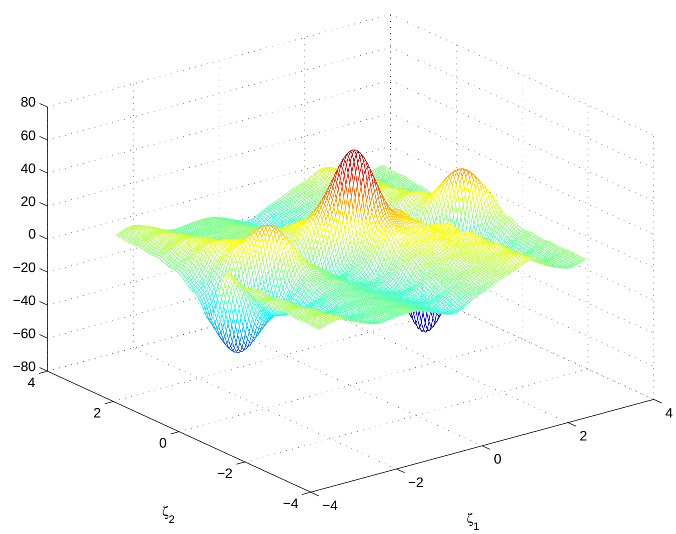

Fig. 9. Shown is the orthogonal projection of the image in Figure 7 onto the sampling space. Only seven samples were taken into account so as to emphasize that this orthogonal projection is analytically known.

form minimax solution. This solution exploits the orthogonal projection induced by the sampling process and it can be implemented by matrix operations (i.e., masking) alone. Such an approach can be incorporated into many multi-dimensional signal processing algorithms where continuous-domain functionals are desired although a sampled version of the signal is the only available data.

ACKNOWLEDGMENTS

This research was supported in part by the HASSIP Research Program HPRN-CT-2002-00285 of the European Commission, and by the Ollendorff Minerva Center. Minerva is funded through the BMBF.

(a) A sampled image.

(b) Gradient values calculated by the minimax approach. Shown are the values raised by 0.4.

(c) Gradient values calculated by the backward difference model. Shown are the values raised by 0.4.

(d) A comparison: minimax approach vs. backward difference model. Shown is the difference image. The values raised by 0.4.

Fig. 10. Gradient approximation: minimax approach vs. backward difference method.

References

[1] M. Fornasier, "Function spaces inclusion and rate of convergence of Riemann-type sums in numerical integration," *Numerical Functional Analysis and Opt.*, vol. 24, no. 1-2, pp. 45–47, 2003.

[2] M. Unser and A. Aldroubi, "A general sampling theory for nonideal acquisition devices," *IEEE Trans. Signal Processing*, vol. 42, no. 11, pp. 2915–2925, Nov. 1994.

[3] Y. C. Eldar, "Sampling and reconstruction in arbitrary spaces and oblique dual frame vectors," *J. Fourier Analys. Appl.*, vol. 1, no. 9, pp. 77–96, Jan. 2003.

[4] G. G. Walter, *Wavelets and Other Orthogonal Systems With Applications*. CRC Press, Boca Raton, FL., 1994.

[5] A. Aldroubi and K. Grochenig, “Non-uniform sampling and reconstruction in shift-invariant spaces,” *SIAM. Rev.*, vol. 43, pp. 585–616, Dec. 2001.

[6] B. Porat, *A Course in Digital Signal Processing*. John Wiley and Sons, Inc., 1997.

[7] S. Angenent, E. Pichon, and A. Tannenbaum, “Mathematical methods in medical image processing,” *Bulletin of the American Mathematical Society*, 2006.

[8] M. Porat and Y. Y. Zeevi, “The generalized Gabor scheme of image representation in biological and machine vision,” *IEEE Trans. on PAMI*, vol. 10, no. 4, December 1988.

[9] Y. Eldar, M. Lindenbaum, M. Porat, and Y. Y. Zeevi, “The farthest point strategy for progressive image sampling,” *IEEE Trans. Image Processing*, vol. 6, pp. 1305–1315, September 1997.

[10] M. N. Do and M. Vetterli, “The contourlet transform: An efficient directional multiresolution image representation,” *IEEE Trans. Image Processing*, vol. 14, pp. 2091–2106, December 2005.

[11] J. L. Starck, M. Elad, and D. L. Donoho, “Image decomposition via the combination of sparse representations and a variational approach,” *IEEE Trans. Image Processing*, vol. 14, pp. 1570–1582, October 2005.

[12] S. Farkash, D. Malah, and W. A. Pearlman, “Transform trellis coding of images at low bit rates,” *IEEE Trans. Commun.*, vol. 38, pp. 1871–1878, October 1990.

[13] M. Elad and A. Feuer, “Super-resolution restoration of continuous image sequence – adaptive filtering approach,” *IEEE Trans. Image Processing*, vol. 8, pp. 387–395, March 1999.

[14] A. M. Bronstein, M. M. Bronstein, M. Zibulevsky, and Y. Y. Zeevi, “Blind deconvolution of images using optimal sparse representations,” *IEEE Trans. Image Processing*, vol. 14, pp. 726–736, June 2005.

[15] ——, “Sparse ICA for blind separation of transmitted and reflected images,” *International J. Imaging Science and Technology*, vol. 15, pp. 84–91, 2005.

[16] K. Sayood, *Introduction to Data Compression*. Morgan Kaufmann (2nd edition), 2000.

[17] F. Meyer, A. Averbuch, and R. Coifman, “Multilayered image representation: Application to image compression,” *IEEE Trans. Image Processing*, vol. 11, pp. 1072–1080, September 2002.

[18] H. Greenspan, M. Porat, and Y. Zeevi, “Projection-based approach to image analysis: pattern recognition and representation in the position-orientation space,” *IEEE Trans. Pattern Analysis and Machine Intelligence*, vol. 14, pp. 1105–1110, November 1992.

[19] C. Sagiv, N. Sochen, and Y. Zeevi, “Integrated active contours for texture segmentation,” *IEEE Trans. Image Processing*, vol. 15, pp. 1633–1646, June 2006.

[20] A. Averbuch, R. Coifman, D. Donoho, M. Elad, and M. Israeli, “Fast and accurate polar Fourier transform,” *to appear in Journal on Applied and Computational Harmonic analysis*.

[21] G. Gilboa, N. Sochen, and Y. Zeevi, “Forward-and-backward diffusion process for adaptive image enhancement and denoising,” *IEEE Trans. on Image Processing*, vol. 11, pp. 689–703, July 2002.

[22] ——, “Image enhancement and denoising by complex diffusion processes,” *IEEE Trans. Pattern Analysis and Machine Intelligence*, vol. 26, pp. 1020–1036, August 2004.

[23] I. Gohberg and S. Goldberg, *Basic Operator Theory*. Boston, MA: Birkhäuser, 1980.

[24] H. Kirshner and M. Porat, “On the approximation of L_2 inner products from sampled data,” *to appear in IEEE Trans. Signal Processing*.

[25] R. A. Adams, *Sobolev spaces*. New York, NY: Academic Press, 1975.

[26] T. G. Dvorkind, H. Kirshner, Y. C. Eldar, and M. Porat, “Minimax approximation of representation coefficients from generalized samples,” Technion CCIT Report 582, April 2006, submitted to *IEEE Trans. Signal Processing*.

[27] A. Aldroubi and M. Unser, “Sampling procedures in function spaces and asymptotic equivalence with shannon’s sampling theory,” *Numer. Funct. Anal. Opt.*, vol. 43, pp. 1–21, Feb. 1994.

[28] M. Unser and J. Zerubia, "Generalized sampling: Stability and performance analysis," *IEEE Trans. Signal Processing*, vol. 45, no. 12, pp. 2941–2950, Dec. 1997.

[29] P. P. Vaidyanathan, "Generalizations of the sampling theorem: Seven decades after Nyquist," *IEEE Trans. Circuit Syst. I*, vol. 48, no. 9, pp. 1094–1109, Sep. 2001.

[30] Y. C. Eldar and T. Dvorkind, "A minimum squared-error framework for sampling and reconstruction in arbitrary spaces," *IEEE Trans. Signal Processing*, vol. 54, no. 6, July 2006.

[31] M. Unser, "Sampling—50 years after Shannon," *IEEE Proc.*, vol. 88, pp. 569–587, April 2000.

[32] ——, "Cardinal exponential splines: part II - think analog, act digital," *IEEE Trans. Signal Processing*, vol. 53, no. 4, pp. 1439 – 1449, Apr. 2005.

[33] H. Kirshner, T. G. Dvorkind, Y. C. Eldar, and M. Porat, "On signal representation from generalized samples: Minmax approximation with constraints," in *EUSIPCO*, 2006.

[34] O. Christensen, "Operators with closed range, pseudo-inverses, and perturbation of frames for a subspace," *Canad. Math. Bull.*, vol. 42, no. 1, pp. 37–45, 1999.

[35] A. Feuer and G. C. Goodwin, "Reconstruction of multi-dimansional bandlimited signals from nonuniform and generalized samples," *IEEE Trans. Signal Processing.*, vol. 53, pp. 4273–4282, November 2005.

[36] E. J. Candes and D. L. Donoho, "Curvelets - a surprisingliy effective non-adaptive representation for objects with edges," in *Curve and Surface Fitting*, A. Cohen and C. Rabut, Eds. Saint Malo: Vanderbilt University, 1999.

[37] M. N. Do and M. Vetterli, "The finite ridgelet transform for image representation," *IEEE Trans. Image Processing*, vol. 12, pp. 16–28, January 2003.

[38] H. G. Feichtinger and T. Strohmer, Eds., *Advances in Gabor Analysis*. Boston, MA: Birkhäuser, 2003.

[39] K. Gröchenig, *Foundations of Time-Frequency Analysis*. Boston, MA: Birkhäuser, 2001.

[40] S. G. Mallat, *A Wavelet Tour of Signal Processing*. San Diego: Academic Press, 1998.

[41] M. Porat and G. Shachor, "Signal representation in the combined phase - spatial space: Reconstruction and criteria for uniqueness," *IEEE Trans. on Signal Processing*, vol. 47, no. 6, pp. 1701–1707, 1999.

[42] I. Cohen, S. Raz, and D. Malah, "Orthonormal shift-invariant wavelet packet decomposition and representation," *Signal Processing*, vol. 57, pp. 251–270, 1997.

[43] J. Canny, "A computational approach to edge detection," *IEEE Trans. Pattern Analysis and Machine Intelligence*, vol. 8, November 1986.

[44] A. K. Jain, *Fundamentals of Digital Image Processing*. Englewood Cliffs, NJ: PRENTICE-HALL, 1989.

[45] R. M. Young, *An Introduction to Nonharmonic Fourier Series*. Academic Press, 2001.

[46] A. Averbuch and V. Zheludev, "A new family of spline-based biorthogonal wavelet transforms and their application to image compression," *IEEE Trans. Image Processing*, vol. 13, pp. 993–1007, July 2004.

[47] A. Averbuch, R. Coifman, D. Donoho, M. Israeli, I. Sedelnikov, and Y. Shkolnisky, "A framework for discrete integral transformations II - the 2D discrete radon transform," January 2006, submitted for publication.